HHS Public Access

Author manuscript

Sci Signal. Author manuscript; available in PMC 2020 December 23.

Published in final edited form as:

Sci Signal. ; 13(637): . doi:10.1126/scisignal.aba1015.

TRPML1 Channels Initiate Ca^{2+} Sparks in Vascular Smooth Muscle Cells

Pratish Thakore[1,†], **Harry A. T. Pritchard**[1,†], **Caoimhin S. Griffin**[1,†], **Evan Yamasaki**[1,†], **Bernard T. Drumm**[2], **Conor Lane**[1], **Kenton M. Sanders**[2], **Yumei Feng Earley**[1,2], **Scott Earley**[1,*]

[1]Department of Pharmacology, Center for Molecular and Cellular Signaling in the Cardiovascular System, University of Nevada, Reno School of Medicine, Reno, Nevada USA 89557-0318

[2]Department of Physiology and Cell Biology, University of Nevada, Reno School of Medicine, Reno, Nevada USA 89557-0318

Abstract

TRPML1 (transient receptor potential mucolipin 1) is a Ca^{2+}-permeable, non-selective cation channel localized to the membranes of endosomes and lysosomes and is not present or functional on the plasma membrane. Ca^{2+} released from endosomes and lysosomes into the cytosol through TRPML1 channels is vital for trafficking, acidification, and other basic functions of these organelles. Here, we investigated the function of TRPML1 channels in fully differentiated contractile vascular smooth muscle cells (SMCs). In live-cell confocal imaging studies, we found that most endosomes and lysosomes in freshly isolated SMCs from cerebral arteries were essentially immobile. Using nanoscale super-resolution microscopy, we found that TRPML1 channels present in late endosomes and lysosomes formed stable complexes with type 2 ryanodine receptors (RyR2) on the sarcoplasmic reticulum (SR). Spontaneous Ca^{2+} signals resulting from the release of SR Ca^{2+} through RyR2s ("Ca^{2+} sparks") and corresponding Ca^{2+}-activated K^+ channel activity are critically important for balancing vasoconstriction. We found that these signals were essentially absent in SMCs from TRPML1-knockout (*Mcoln1*$^{-/-}$) mice. Using ex vivo pressure myography, we found that loss of this critical signaling cascade exaggerated the vasoconstrictor responses of cerebral and mesenteric resistance arteries. In vivo radiotelemetry studies showed that *Mcoln1*$^{-/-}$ mice were spontaneously hypertensive. We conclude that TRPML1 is crucial for the initiation of Ca^{2+} sparks in SMCs and the regulation of vascular contractility and blood pressure.

[*]To whom correspondence should be addressed: Scott Earley, Ph.D., University of Nevada, Reno School of Medicine, Manville Health Sciences Building, Room 8, MS-0318, Reno, NV 89557-0318, USA, Phone: (775) 784-4117; searley@med.unr.edu.
[†]These authors contributed equally to this work.

Author contributions: S.E. initiated and supervised the project and designed experiments. E.Y. performed RT-qPCR and Wes protein detection experiments. E.Y. and C.L. performed LysoTracker live-cell confocal microscopy experiments. C.S.G., H.A.T.P, and E.Y. performed super-resolution imaging experiments. B.T.D. conducted and analyzed Ca^{2+} spark recordings. H.A.T.P and E.Y. performed patch-clamp electrophysiology experiments. P.T. performed pressure myography experiments. P.T. and Y.F.E. performed in vivo BP recording studies. P.T., C.S.G., H.A.T.P, and S.E. analyzed the data. S.E. wrote the manuscript and prepared the figures. P.T., H.A.T.P, Y.F.E., K.M.S., and S.E. revised the manuscript.

Competing interests: The authors declare that they have no competing interests.

Data and materials availability: All data needed to evaluate the conclusions in the paper are present in the paper or the Supplementary Materials.

Introduction

The transient receptor potential mucolipin (TRPML) subfamily of Ca^{2+}-permeable, non-selective cation channels consists of three members, TRPML1, TRPML2 and TRPML3, encoded by the genes *Mcoln1*, *Mcoln2* and *Mcoln3*, respectively (1, 2). TRPML1 channels are broadly distributed (3), whereas TRPML2 is expressed at high levels only in lymphoid and myeloid tissues (4, 5), and TRPML3 is most abundant in the cochlea and in melanocytes (6). TRPML channels are not expressed at high levels on the plasma membrane, and instead are mainly localized to the membranes of late endosomes and lysosomes (LELs). Channel activity is potentiated by acidic pH (6, 7) and depends on phosphatidylinositol 3,5-bisphosphate ($PtdIns(3,5)P_2$), a phosphoinositide species that is abundant in the membranes of LELs, but rare within the plasma membrane (8). TRPML channels are important for many of the canonical functions of LELs, including H^+ homeostasis (9), maturation, fusion, trafficking (1), and autophagy (10–12). Here, we explored an unorthodox role for TRPML channels in the regulation of Ca^{2+} signaling mechanisms and contractility of native vascular smooth muscle cells (SMCs).

The contractile state of SMCs is determined by a complex interplay of global and localized Ca^{2+} signaling mechanisms. Vasoconstriction is caused by membrane depolarization-dependent Ca^{2+} influx through voltage-dependent $Ca_V1.2$ channels, which elevates overall cytosolic [Ca^{2+}] in SMCs (13). In contrast, the effects of localized, transient changes in intracellular [Ca^{2+}] that occur within specific subcellular compartments are more nuanced. Such signals are exemplified by Ca^{2+} sparks—large-amplitude, transient Ca^{2+}-signaling events that reflect the optically detected release of Ca^{2+} through clusters of type 2 ryanodine receptors (RyR2s) on the sarcoplasmic reticulum (SR) (14). A single Ca^{2+} spark stimulates a functionally coupled cluster of large-conductance Ca^{2+}-activated K^+ (BK) channels on the plasma membrane, giving rise to large outward K^+ currents, membrane hyperpolarization, SMC relaxation, and vasodilation (14, 15). The intraluminal [Ca^{2+}] of LELs (~0.5–2 mM) (16) is much higher than that of the surrounding cytosol (~100–300 nM) of SMCs, and we predict that the opening of Ca^{2+}-permeable TRPML channels on the membrane of LELs will produce transient, localized Ca^{2+} signals. Because the amplitude of an intracellular Ca^{2+} signal originating from a point source rapidly diminishes with distance from the origin, the specific functions of such signals are dictated by the local molecular environment.

In the current study, we tested the hypothesis that TRPML1 channels on LELs influence Ca^{2+} signaling pathways and contractile functions of SMCs. Molecular studies demonstrated that TRPML1 was the only detectable member of the TRPML subfamily in native contractile SMCs. Focusing on this channel, we used a live-cell LEL-tracking assay and nanoscale super-resolution microscopy to establish that TRPML1 and RyR2 formed a stable, closely coupled complex in native SMCs. High-speed confocal Ca^{2+} imaging and patch-clamp electrophysiological studies revealed that spontaneous Ca^{2+} sparks and associated BK channel currents were essentially absent in contractile SMCs isolated from mice with a global deficiency of TRPML1 (*Mcoln1*$^{-/-}$). Arteries from *Mcoln1*$^{-/-}$ mice studied ex vivo were hypercontractile, likely due to loss of RyR2 activity and hyperpolarizing BK channel currents. Experiments performed in vivo using surgically implanted radiotelemetry transmitters revealed that *Mcoln1*$^{-/-}$ mice were spontaneously hypertensive. We conclude

that under physiological conditions TRPML1 channels initiate Ca^{2+} sparks, thereby diminishing SMC contractility to regulate vascular resistance and blood pressure.

Results

TRPML1 channels are present in native vascular SMCs

Expression of *Mcoln1*, *Mcoln2*, and *Mcoln3* in native contractile cerebral artery SMCs was surveyed at the mRNA level using quantitative reverse transcription-polymerase chain reaction (RT-qPCR). Homogeneous populations of native SMCs were obtained from cerebral arteries isolated from $smMHC^{Cre/eGFP}$ reporter mice (17) by enzymatic dispersion and fluorescence-activated cell sorting (FACS), as previously described (18). RT-qPCR data were normalized to expression of the housekeeping gene *Actb*, encoding β-actin. *Mcoln1* was highly expressed in SMCs; in contrast, *Mcoln2* and *Mcoln3* were not present in these samples (Figure 1A), but were readily detectable in positive control RNA (Fig. S1A and B). An analysis of RNA from whole cerebral and mesenteric arteries revealed a similar pattern, with *Mcoln1* expressed at much higher levels compared with *Mcoln2* and *Mcoln3* in vessels from wild-type (WT) animals (Figure 1B and C). We also found that *Mcoln1* was undetectable in arteries from $Mcoln1^{-/-}$ mice and that expression levels of *Mcoln2* and *Mcoln3* did not differ between WT and $Mcoln1^{-/-}$ mice (Figure 1B and C). Using the Wes capillary electrophoresis protein detection system, we identified a single band at the expected molecular weight for TRPML1 (~60 kDa) in cerebral arteries from WT mice, but not in arteries from $Mcoln1^{-/-}$ mice (Figure 1D). We conclude that TRPML1 is the only TRPML subfamily member present in contractile SMCs and that *Mcoln1* knockout does not alter expression levels of *Mcoln2* or *Mcoln3*.

The majority of LELs in contractile SMCs are immobile

TRPML1 channels reportedly contribute to the intracellular trafficking of LELs (1). To investigate the mobility of these organelles in contractile SMCs, we labeled freshly isolated cerebral artery SMCs from WT mice with LysoTracker Deep Red, a dye that specifically stains the membranes of LELs (19). LysoTracker-labeled native contractile SMCs isolated from WT mice (Figure 2A) were imaged using live-cell spinning-disk confocal microscopy, and recordings were analyzed for movement of LysoTracker-labeled structures using NIH Image J. Unexpectedly, we found that the majority of LELs in contractile SMCs isolated from WT mice were essentially immobile, moving less than 1 μm during the recording period (Figure 2B and C; Movie S1). We also found that the majority of LELs in intact pressurized cerebral arteries were also essentially immobile, moving less than 1 μm during the recording period (Fig. S2A to C; Movie S2). We compared these data to those obtained from primary, unpassaged, proliferative cerebral artery SMCs derived from the same animals that had been used for native cell studies and cultured in the presence of serum for 6 days. Cells cultured under these conditions expressed the SMC markers smooth muscle α-actin and myosin heavy chain 11 (Fig. S3A and B). Proliferative SMCs isolated from WT mice were loaded with LysoTracker and imaged under the same conditions used for contractile SMCs (Figure 2D). These live-cell imaging studies revealed that nearly all LELs in proliferative SMCs isolated from WT mice were mobile, exhibiting slow, Brownian-type

diffusion within the cytosol as well as rapid long-range movements along linear tracks (Figure 2E and F; Movie S3).

Using the same procedures, we also examined LEL mobility in native contractile SMCs isolated from *Mcoln1*$^{-/-}$ mice (Figure 2G). Similar to contractile SMCs isolated from WT mice, we found that the majority LELs in contractile SMCs isolated from *Mcoln1*$^{-/-}$ mice were also essentially immobile (Figure 2H and I). Live-cell imaging studies of proliferative SMCs isolated from the same *Mcoln1*$^{-/-}$ mice loaded with LysoTracker (Figure 2J) revealed that LELs in these cells were mobile (Figure 2K and L) but exhibited less mobility compared to proliferative SMCs isolated from WT mice. The mean displacement (Figure 2M) and speed (Figure 2N) of LysoTracker-labeled particles were greater in proliferative SMCs compared to contractile SMCs isolated from both WT and *Mcoln1*$^{-/-}$ mice. In agreement with previous reports of the pivotal role of TRPML1 channels in the trafficking of LELs (1), we observed a marked decrease in mean displacement and speed of LysoTracker-labeled particles in SMCs isolated from *Mcoln1*$^{-/-}$ mice in comparison to corresponding SMCs isolated from WT mice (Figure 2M and N). The density of labeled particles per cell was also greater in proliferative SMCs isolated from both WT and *Mcoln1*$^{-/-}$ mice although deficiency in TRPML1 did not alter the number of labeled particles per cell (Figure 2O). These data suggest that LELs are essentially immobile in fully differentiated contractile SMCs and that reversion to the proliferative phenotype greatly increases the mobility of these organelles. Our data also show that TRPML1 channels contribute to the mobility of LELs in cultured cells.

Lamp-1-positive LELs and TRPML1 are located within 40 nm of RyR2 clusters in native SMCs

The near-immobility of the bulk of LELs in contractile SMCs suggests that these organelles form stable complexes and can functionally interact with neighboring structures. To examine this concept, we determined the subcellular localization of TRPML1 channels relative to RyR2s and the LEL marker protein, Lamp-1 (lysosomal-associated membrane protein 1), in native SMCs using GSDIM (ground-state depletion followed by individual molecule return) super-resolution microscopy (20–22). The specificity of our TRPML1 antibody was validated in Wes protein-detection experiments (Figure 1D) and in control experiments comparing the super-resolution labeling density of cerebral arterial SMCs from WT and *Mcoln1*$^{-/-}$ mice immunolabeled with the TRPML1 primary antibody and secondary antibodies with that of SMCs labeled with the secondary antibody alone (Fig. S4A to C). The specificity of Lamp-1 and RyR2 antibodies was also validated using this latter approach (Fig. S4D to I). The spatial resolution limits of our GSDIM system were probed using 20- and 40-nm DNA-PAINT–based nanorulers (23). GSDIM imaging revealed that the distance between markers for the 40-nm nanoruler was 39 ± 12 nm (mean ± SD), and the full width at half maximum (FWHM) for individual fluorophores was 16 ± 5 nm (Fig. S5A and B). The distance between markers for the 20-nm nanoruler was 23 ± 9 nm, and the FWHM was 11 ± 3 nm (Fig. S5C and D). These values are consistent with those reported in prior studies (24, 25) and demonstrate that the lateral resolution limit of our GSDIM system is between 20 and 40 nm.

Native SMCs were co-immunolabeled for TRPML1 and Lamp-1, RyR2 and Lamp-1, or TRPML1 and RyR2, and imaged using GSDIM in the epifluorescence illumination mode. Super-resolution localization maps showed that TRPML1, Lamp-1, and RyR2 proteins were non-homogeneously distributed and were present as defined clusters in native SMCs (Figure 3A to C). The mean area of TRPML1 protein clusters was smaller than that of RyR2 protein clusters; the sizes of individual clusters of both proteins were exponentially distributed (Figure 3D and E); and the mean density of RyR2 clusters was greater than that of TRPML1 clusters (Figure 3F). High-resolution electron cryomicroscopy structural analyses estimated that the diameter of a single human TRPML1 channel is 10.5 nm (26). Using this value and assuming maximum packing density, we calculated that median-sized TRPML1 protein clusters (1608 nm^2) could contain up to 18 TRPML1 channels.

Individual Lamp-1 protein clusters were organized into larger ovoid metastructures that were between 30,000 and 800,000 nm^2 in size (Figure 3G). This distribution is consistent with the previously reported sizes of LELs (27). Using object-based analysis on cells co-immunolabeled for Lamp-1 and TRPML1, we found that TRPML1 protein clusters colocalized at the resolution limit of our system (20-40 nm) with most (74.5%; 123/165) of the Lamp-1-positive metastructures.

The distance between individual RyR2 clusters and the outer edge of Lamp-1-positive LELs was determined by nearest-neighbor analysis of super-resolution images obtained from cells co-immunolabeled for Lamp-1 and RyR2 (Figure 3B). A plot of the distribution of these data showed that RyR2 clusters were most frequently located between 0 and 40 nm of Lamp-1-positive ovoids, and were randomly assorted at distances of 50 to 500 nm (Figure 3H). These data suggest that RyR2s clusters are most frequently located within 40 nm of Lamp-1-positive LELs in contractile SMCs (288 of 1409 RyR2 clusters) and are randomly distributed relative to LELs outside of this range.

Object-based analysis of super-resolution localization maps of SMCs co-immunolabeled for TRPML1 and RyR2 showed that a significantly greater fraction of TRPML1 protein clusters colocalized with RyR2 clusters compared with a simulated random distribution (Figure 3I). These data indicate that a population of TRPML1 channels are located less than 40 nm from RyR2s in contractile SMCs. Together, our data support the concept that TRPML1 channels in Lamp-1-positive LELs form stable complexes with RyR2s in contractile SMCs.

SMCs from Mcoln1$^{-/-}$ mice lack spontaneous Ca^{2+} sparks and BK channel activity

Ca^{2+} sparks were recorded in contractile cerebral artery SMCs isolated from WT and *Mcoln1*$^{-/-}$ mice using spinning-disk confocal microscopy (Figure 4A and B). Spontaneous Ca^{2+} sparks were present in nearly all SMCs (11/13) obtained from WT mice, but were detected in less than 11% of SMCs obtained from *Mcoln1*$^{-/-}$ mice. Further, the number of Ca^{2+} spark sites per cell and the mean frequency of Ca^{2+} sparks were considerably lower in SMCs from *Mcoln1*$^{-/-}$ mice compared with controls (Figure 4C and D). A comparison of total SR Ca^{2+} store load between groups, performed by recording changes in global [Ca^{2+}] in response to caffeine (10 mM) pulses, demonstrated that there were no differences between SMCs from WT and *Mcoln1*$^{-/-}$ mice (Figure 4E). These data show that the lack of

spontaneous Ca^{2+} spark activity in SMCs from *Mcoln1*$^{-/-}$ mice is not due to differences in SR [Ca^{2+}].

Ca^{2+} sparks activate clusters of BK channels on the plasma membrane, generating large-amplitude spontaneous transient outward currents (STOCs) (14). In native cerebral artery SMCs voltage-clamped at a physiologically relevant membrane potential (−40 mV), STOCs were present in cells obtained from WT animals but were almost undetectable in SMCs from *Mcoln1*$^{-/-}$ mice (Figure 5A). Mean STOC frequency and amplitude were lower in SMCs from *Mcoln1*$^{-/-}$ mice compared with WT mice over a range of membrane potentials (Figure 5B and C). In control studies, we found that whole-cell BK current density did not differ between SMCs from WT and *Mcoln1*$^{-/-}$ mice, suggesting that TRPML1 knockout did not alter the number of BK channels available for activation at the plasma membrane (Fig. S6A and B). We also found that mRNA expression of *Ryr2* (encoding RyR2), *Kcnma1* (encoding the BKα pore-forming subunit), and *Kcnmb1* (encoding the BK β1 regulatory subunit) did not differ between WT and *Mcoln1*$^{-/-}$ mice (Fig. S6C). The mobility of LELs in proliferative SMCs suggests that these cells might lack stable TRPML1-RyR2-BK signaling complexes. To test this hypothesis, we recorded STOC activity in proliferative SMCs using perforated patch-clamp electrophysiology. STOC frequency essentially 0 at membrane potentials that are physiologically-relevant for native SMCs (−60 to −20 mV and minimal at more depolarized membrane potentials (Fig. S7A to C). These data further support the concept that the formation of stable signaling complexes between TRPML1 channels on LELs and the RyR2-BK signaling cascade is necessary for the generation of STOCs.

To further characterize the impact of *Mcoln1* knockout on spontaneous BK channel activity, we used a pharmacological approach. We found that the selective TRPML channel agonist MK6-83 (28) significantly increased STOC frequency in SMCs from WT, but not those from *Mcoln1*$^{-/-}$ mice (Figure 5D and E). However, STOC amplitude was not affected by MK6-83 in both WT and *Mcoln1*$^{-/-}$ mice (Fig. S8). TRPML1 channel activity is regulated by intravesicular pH (6, 7). Therefore, we predicted that disruption of LEL pH by inhibiting the vacuolar H^+-ATPase would diminish TRPML1 activity and reduce STOCs. We found that STOC frequency was nearly abolished by treating native SMCs with the vacuolar H^+-ATPase inhibitor bafilomycin A1 (Baf-A1) (Fig. S9A and B) and that STOC amplitude was significantly reduced by this treatment (Fig. S9C). Baf-A1 did not affect whole-cell BK channel currents (Fig. S9D and E). In additional control experiments, we treated voltage-clamped SMCs with GSK1016790A, a selective activator of TRP vanilloid 4 (TRPV4) channels (29), to engage an independent signaling cascade that stimulates increases in Ca^{2+} spark and STOC frequency through TRPV4-mediated Ca^{2+} influx and Ca^{2+}-induced Ca^{2+} release from RyR2s (30, 31). These experiments showed that stimulation of TRPV4 channels increased STOC frequency, but not amplitude, to a similar extent in SMCs from WT and *Mcoln1*$^{-/-}$ mice (Figure 5F and G, Fig. S10), demonstrating that TRPML1 knockout does not result in off-target effects that prevent pharmacological engagement of the Ca^{2+} spark/BK pathway. We conclude that TRPML1 expression is necessary for spontaneous activity of the Ca^{2+} spark/BK channel signaling cascade in contractile SMCs.

Resistance arteries from Mcoln1$^{-/-}$ mice are hypercontractile

The involvement of TRPML1 channels in the regulation of vascular contractility was investigated in a series of ex vivo pressure myography experiments. We found that arteries isolated from *Mcoln1*$^{-/-}$ mice constricted more robustly in response to increases in intraluminal pressure within the physiological range compared with cerebral arteries (Figure 6A and B). In addition, cerebral arteries from *Mcoln1*$^{-/-}$ mice were more sensitive to the constrictive effects of the thromboxane A_2 receptor agonist U46619 (Figure 6C and D) compared with arteries from WT mice. Similarly, the contractile response to increase in intraluminal pressure was greater in mesenteric arteries from *Mcoln1*$^{-/-}$ mice (Figure 6E and F), as was the contractile response to the α_1-adrenergic receptor agonist phenylephrine (Figure 6G and H). In control studies, we found that the degree of constriction of cerebral (Fig. S11A) and mesenteric (Fig. S11B) arteries induced by elevating extracellular [K^+] to 60 mM did not differ between arteries isolated from WT and *Mcoln1*$^{-/-}$ mice, indicating that loss of TRPML1 expression did not grossly alter voltage-dependent Ca^{2+} influx or contractile pathways associated with direct depolarization of the SMC plasma membrane. In addition, we found that vasodilation in response to the nitric oxide donor sodium nitroprusside did not differ between cerebral arteries isolated from WT and *Mcoln1*$^{-/-}$ mice (Fig. S12).

Mcoln1$^{-/-}$ mice are hypertensive

Age- and size-matched WT and *Mcoln1*$^{-/-}$ mice were surgically implanted with radio telemetry transmitters as previously described (32). After a recovery period (14 days), systolic and diastolic blood pressure (BP) and heart rate were recorded for 48 hours. Normal diurnal variations were observed for all parameters. The mean systolic BP of *Mcoln1*$^{-/-}$ mice was greater than that of WT mice during both day and night cycles (Figure 7A and B), whereas diastolic BP did not differ between groups (Figure 7C and D). Mean arterial pressure (MAP) (Figure 7E and F) was also greater in *Mcoln1*$^{-/-}$ mice compared with WT mice, whereas heart rate (Fig. S13A and B) and locomotor activity (Fig. S13C and D) did not differ between groups. These data indicate that knockout of TRPML1 results in spontaneous systolic hypertension, which is associated with elevated arterial contractility and decreased compliance in human patients (33). Regulation of BP is influenced by the central and autonomic nervous systems and the kidneys in addition to peripheral resistance imparted by small blood vessels. Our data suggest that elevated SMC contractility and excessive constriction of arteries from *Mcoln1*$^{-/-}$ mice contributes to elevated BP in these animals.

Discussion

Vascular resistance is primarily determined by the diameter of small arteries and arterioles, and its dynamic regulation by relaxation or contraction of SMCs controls blood flow and pressure. Here, we provide evidence that the activity of TRPML1, a non-selective cation channel localized to LELs, diminished SMC contractility, vasoconstrictor responsiveness, and BP. Using live-cell imaging and super-resolution microscopy, we showed that TRPML1 channels in LELs formed stable, closely coupled complexes with RyR2s in contractile SMCs. Our findings also indicated that TRPML1 was required for the generation of

spontaneous Ca^{2+} sparks and corresponding BK channel activity. Failure to initiate this vital signaling cascade in *Mcoln1*$^{-/-}$ mice resulted in excessive vasoconstriction and was associated with the development of hypertension. We conclude that TRPML1 is critically important for initiation of Ca^{2+} sparks in SMCs and the consequent control of arterial tone.

The Ca^{2+} spark/BK channel signaling pathway is a fundamental regulator of vascular tone. BK channel currents, which are stimulated by spontaneous Ca^{2+} sparks, control SMC membrane potential and contractility (14, 34, 35), and provide critical negative feedback that limits the extent and duration of vasoconstrictor responses (15). Genetic knockout of the BK channel β1 subunit, a regulatory subunit that enhances the Ca^{2+} sensitivity of the channel (36), causes excessive vasoconstriction, elevated total vascular resistance, and hypertension (34, 35). Functional uncoupling of Ca^{2+} sparks from BK channels due to downregulation of the β1 subunit is associated with hypertension in human patients (37, 38). Conversely, a gain of function mutation in *KCNMB1*, which encodes the β1 subunit, is associated with lower than expected rates of diastolic hypertension in humans, providing evidence of the pathophysiological impact of this pathway (39). Our data showed that TRPML1 channels, acting upstream of RyR2s, were necessary for the spontaneous generation of Ca^{2+} sparks. Further, we found that knockout of TRPML1 in mice had an effect similar to that of knocking out the BK β1 subunit—specifically, exaggerated vasoconstrictor responses and hypertension. Thus, our findings identify TRPML1 as an essential component of the vital Ca^{2+} spark/BK signaling cascade in contractile SMCs.

How does TRPML1 stimulate the generation of Ca^{2+} sparks? We propose a model based on the localization of the channel within contractile SMCs. LELs are highly mobile in many types of cells, including proliferative SMCs, but our data showed that the vast majority of these organelles were essentially immobile in contractile SMCs. Further, a substantial population of TRPML1 channel clusters on the membranes of LELs was localized to within less than 40 nm of RyR2s on the SR in native SMCs. Because of the steep Ca^{2+} gradient between the lumen of LELs and the cytosol (16), the opening of TRPML1 channels is predicted to create a Ca^{2+} microdomain near the mouth of the channel (40). We propose that Ca^{2+} released from LELs through TRPML1 channels that are closely coupled with RyR2s triggers Ca^{2+} sparks through Ca^{2+}-induced Ca^{2+} release. In this manner, a Ca^{2+}-release event initiated by TRPML1 is amplified by Ca^{2+} released through RyR2s to generate a Ca^{2+} spark and activate subsequent downstream signaling events. Sustaining the activity of this pathway requires that the intraluminal [Ca^{2+}] of an LEL proximal to an individual RyR2 cluster be restored prior to the initiation of another Ca^{2+} spark at that site. The mechanisms that establish the Ca^{2+} gradient between the LEL lumen and cytosol are not known, but the involvement of an unidentified H^+/Ca^{2+} exchanger has been proposed (16). It is conceivable that a fraction of the Ca^{2+} released from the SR through RyR2s is taken up by LELs and then later released to trigger a subsequent Ca^{2+} spark, contributing to the formation of a self-sustaining Ca^{2+} signaling oscillator.

The specific properties of TRPML1 have been investigated by patch-clamp electrophysiology using cells overexpressing a TRPML1 variant containing a specific point mutation that promotes trafficking of the channel to the plasma membrane (6) and by treating cultured cells with vacuolin-1 to enlarge LELs (7). These studies showed that

TRPML channel activity is potentiated by acidic conditions and is specifically activated by the phosphoinositide PtdIns(3,5)P_2 (8), which is abundant in the membranes of LELs. We predict that acidification of endosomes and the abundance of PtdIns(3,5)P_2 in the membrane of these vesicles promotes frequent stochastic openings of TRPML1 channels that may be responsible for triggering spontaneous Ca^{2+} sparks in contractile SMCs. In addition, TRPML1 channels are sensitized or activated by exogenous oxidants and endogenously generated reactive oxygen species (ROS) (11), and inhibited by the mammalian target of rapamycin (mTOR) (41). We attempted to study the role of ROS and mTOR regulation of TRPML1 in contractile SMCs. However, in preliminary experiments, we found that, although vacuolin-1 increased the size of LELs in HEK cells, this treatment did not enlarge these organelles in native SMCs. These findings are in agreement with those of a prior study reporting that vacuolin-1 treatment does not increase the size of LELs in primary dorsal root ganglion neurons (42) and suggest that the effects of this compound are cell-type specific. As a consequence, we are unable to analyze TRPML1 regulation in contractile SMCs using patch-clamp electrophysiology. TRPML1 activity can also be studied in cultured cells that express Ca^{2+}-biosensor proteins targeted to LELs (43). However, because SMCs rapidly undergo phenotypic changes under cell culture conditions (44), application of this method to study TRPML1-dependent Ca^{2+} signaling in fully differentiated contractile SMCs will require the development of new transgenic mice expressing LEL-targeted Ca^{2+} biosensors.

Loss-of-function mutations in *MCOLN1* are associated with mucolipidosis type IV (MLIV) (3, 45), an extremely rare human lysosomal storage disease, with just over 100 reported cases (46). MLIV patients exhibit delayed development of mental and motor skills, impaired vision, achlorhydria and other pathologies in multiple organ systems (47), many of which are recapitulated in *Mcoln1*$^{-/-}$ mice (48). Ultrastructural skin biopsies of MLIV patients have revealed abnormalities in blood vessel walls and smooth muscle fibers (49), but none of the clinical studies have reported hypertension. This may be because nearly all of the case studies describe the disease in children or young adults, before cardiovascular pathology becomes evident.

The Ca^{2+} spark/BK channel signaling pathway was first described in SMCs more than two decades ago (14), but the initiation of these seemingly spontaneous Ca^{2+} signals has remained enigmatic. Our study demonstrates that TRPML1 channels act upstream of RyR2s in this pathway and are necessary for the generation of spontaneous Ca^{2+} sparks and subsequent activation of BK channels. Knockout of *Mcoln1* resulted in vascular hypercontractility and hypertension, effects similar to those of knocking out a BK channel regulatory subunit (34, 35). We conclude that TRPML1 is critically important for the regulation of vascular contractility.

Materials and Methods

Chemical and reagents

All chemicals and reagents were obtained from Sigma-Aldrich (St. Louis, MO, USA), unless stated otherwise.

Animals

Adult (16–20 weeks of age) male WT C57BL/6J mice (Jackson Laboratories, Bar Harbor, ME, USA), homozygous global *Mcoln1*$^{-/-}$ mice (B6.Cg-Mcoln1^{tm1Sasl}/J, strain #027110; Jackson Laboratory), and *smMHC*$^{Cre/eGFP}$ (B6.Cg-Tg[Myh11-cre-EGFP]2Mik/J) reporter mice that express eGFP exclusively in SMCs under the control of the myosin heavy chain promoter (17) were used for these studies. Animals were maintained in individually ventilated cages (<5 mice/cage) with ad libitum access to food and water, in a room with controlled 12-hour light and dark cycles. All animal care procedures and experimental protocols involving animals were performed in compliance with the NIH *Guide for the Care and Use of Laboratory Animals* and were approved by the Institutional Animal Care and Use Committee at the University of Nevada, Reno School of Medicine. Arteries for ex vivo experimentation were harvested from mice that were deeply anaesthetized with isoflurane (Baxter Healthcare, Deerfield, IL, USA) and euthanized by decapitation and exsanguination. Brains and mesenteries were isolated and placed in ice-cold Ca^{2+}-free physiological saline solution (Ca^{2+}-free PSS; 134 mM NaCl, 5 mM KCl, 2 mM $MgCl_2$, 10 mM HEPES, 10 mM glucose, 0.5% bovine serum albumin [BSA], pH 7.4).

Enzymatic dispersal of SMCs

Individual native SMCs were obtained by digesting freshly isolated arteries in papain (1 mg/ml; Worthington Biochemical Corporation, Lakewood, NJ, USA), dithiothreitol (1 mg/ml), and BSA (10 mg/ml) in Ca^{2+}-free PSS at 37°C for 12 minutes, followed by a 14-minute incubation in type II collagenase (1 mg/ml; Worthington Biochemical Corporation). Digested arteries were washed with Ca^{2+}-free PSS and triturated with a polished glass pipette to dissociate SMCs. SMCs were freshly dissociated on the day of experiments.

Isolation of SMCs using fluorescence-activated cell sorting (FACS)

Native cerebral artery SMCs were isolated from *smMHC*$^{Cre/eGFP}$ reporter mice using previous described protocols (18, 50). Briefly, after enzymatically dispersing as described above, eGFP-expressing cells were sorted by FACS using a BD Biosciences FACSAria II flow cytometer (San Jose, CA, USA) with a 130-μm nozzle at a sheath pressure of 12 psi. Viability was assessed by labeling cells with Hoechst 33258 (1 μg/ml) followed by excitation with a 355-nm UV laser and emission detection using a 450/50 nm bandpass filter. Cells with compromised membranes that stained positively for Hoechst 33258 were eliminated. Cells that were negative for Hoechst 33258 but positive for eGFP (488 nm excitation) were collected in a tube containing TRIzol reagent (Invitrogen, Carlsbad, CA, USA) and further processed for RNA isolation. FACS was performed in the FACS/FCMSRL Core Facility at the University of Nevada, Reno School of Medicine.

RNA isolation and RT-PCR

Cerebral and mesenteric arteries or FACS-isolated SMCs were placed into TRIzol Reagent (Invitrogen) and homogenized using a syringe and 20-gauge needle. The homogenate was centrifuged at 20,800 × g for 5 minutes, and the RNA-containing supernatant was transferred to a new tube. Total RNA was isolated using Direct-zol RNA MicroPrep (Zymo Research, Irvine, CA, USA), quantified using a Nanodrop 2000 spectrophotometer

(ThermoFisher, Waltham, MA, USA), and treated with OPTIZYME DNase I (Fisher BioReagents, Pittsburgh, PA, USA). First-strand cDNA was synthesized using qScript cDNA SuperMix (Quanta, Gaithersburg, MD, USA).

RT-qPCR was performed on a QuantStudio 3 system (ThermoFisher) using Fast SYBR Green Master Mix (ThermoFisher) and specific custom-designed primers (Table S1). The efficiency of RT-qPCR primer pairs (Fig. S1) for *Mcoln1*, *Mcoln2*, and *Mcoln3* was determined using serial dilations of first-strand cDNA generated from Mouse XpressRef Universal Total RNA (Qiagen), which also served as positive control material for all assays. Reactions without template cDNA served as contamination controls. RT-qPCR data were normalized to β-actin and analyzed using the ΔΔCT method (51).

Endpoint RT-PCR was performed using GoTaq Green Master Mix (Promega, Madison, WI, USA) and the specific primer pairs indicated above in a T100 Thermal Cycler (Bio-Rad, Hercules, CA, USA). PCR products were resolved on 2% agarose gels containing ethidium bromide and imaged on a Bio-Rad Chemidoc (Bio-Rad).

Protein extraction and Wes protein analysis

Arteries were isolated, cut into small segments, and placed directly into ice-cold 1× RIPA buffer (Cell Biolabs, San Diego, CA, USA) supplemented with 1% protease inhibitor cocktail (Cell Biolabs). Following a 15 minute incubation, samples were disrupted using a hand-held homogenizer equipped with a sterile disposable tip (VWR, Radnor, PA, USA) and further processed using a probe sonicator (Fisher Scientific, Hampton, NH, USA). Homogenized samples were centrifuged at 20,800 × *g* for 20 min at 4 °C, and the supernatant was transferred to a clean tube. The protein concentration of the supernatant was determined using a Pierce BCA Protein Assay Kit (ThermoFisher), and absorbance values were read using a FlexStation 3 plate reader (Molecular Devices, San Jose, CA, USA).

Protein expression was measured using a Wes automated capillary-based protein detection system (ProteinSimple, Santa Clara, CA, USA) employing 25-capillary 12 to 230-kDa Wes separation modules and anti-mouse/rabbit detection modules, according to the manufacturer's recommendations. Briefly, samples (0.3 mg/mL) were diluted in a fluorescence-reducing buffer and heated to 95 °C for 5 min before loading onto the Wes plate. A biotinylated ladder was included in all Wes experiments. Rows were successively loaded with Wes antibody diluent blocking buffer; anti-TRPML1 (1:50, sc-398868, Santa Cruz Biotechnology, Santa Cruz, CA, USA) or anti–β-actin (1:1000, ab8227, Abcam, Cambridge, MA, USA), horseradish peroxidase (HRP)-conjugated anti-mouse or -rabbit secondary antibody (1×; ProteinSimple), and a luminol–peroxide mix. Data were analyzed using Compass for SW (ProteinSimple).

Primary SMC culture

Enzymatically dispersed cerebral artery SMCs were cultured as previously described (52) on 30-mm glass-bottomed culture dish in Complete Smooth Muscle Cell Growth Medium (Cell Biologics, Inc., Chicago, IL, USA) in an incubator maintained at 37°C with 6% CO_2. SMCs were cultured for 6 days prior to study; some cultures were immunolabeled for smooth

muscle α-actin (ab5694, 1:100, Abcam) and myosin heavy chain (ab53219, 1:100, Abcam) expression (Fig. S3).

LysoTracker

Freshly isolated cerebral artery SMCs and cultured proliferative SMCs were labeled with LysoTracker Deep Red (50 nM; ThermoFisher) diluted in Ca^{2+}-free PSS for 30 minutes at room temperature (22°C). Labeled cells were then washed with and maintained in HEPES buffered imaging solution (146 mM NaCl, 4.7 mM KCl, 0.6 mM $MgSO_4$, 0.15 $NaHPO_4$, 2.5 mM $CaCl_2$, 8 mM glucose, 0.1 mM ascorbic acid, 10 mM HEPES, pH 7.4). Cells were imaged using a custom built live-cell spinning-disk confocal microscopy (laser source, Andor Integrated Laser Engine, Andor Technology, Belfast, UK; spinning disk CSU-X1, Yokogawa, Tokyo, Japan; inverted microscope IX81, Olympus, Tokyo, Japan). Images were obtained using a 100x (NA 1.45) oil-immersion lens (Olympus) and an electron multiplying charge-coupled device (EMCCD) camera (iXon 897, Andor Technology) using μManager software (version 1.4, Vale Lab, UCSF, San Francisco, CA, USA).

Intact cerebral arteries were labeled with LysoTracker Deep Red (50 nM; ThermoFisher) diluted in DMEM (ThermoFisher) for 1 hour at 37°C with 6% CO_2. Arteries were mounted between two glass pipettes (outer diameter, 40-50 μm) in a pressure myograph chamber (Living Systems Instrumentation, Burlington, VT, USA) and secured by nylon thread. Intraluminal pressure was controlled using a servo-controlled peristaltic pump (Living Systems Instrumentation). Arteries were bathed in warmed (37°C), oxygenated (21% O2, 6% CO2, 73% N2) PSS (119 mM NaCl, 4.7 mM KCl, 21 mM NaHCO3, 1.17 mM MgSO4, 1.8 mM CaCl2, 1.18 mM KH2PO4, 5 mM glucose, 0.03 mM EDTA) at an intraluminal pressure of 5 mmHg. Following a 15-minute equilibration period, intraluminal pressure was increased to 110 mmHg and vessels were stretched to their approximate in vivo length, after which pressure was reduced back to 5 mmHg for an additional 15 minute equilibration period. Intraluminal pressure was then increased to 20 mmHg to and arteries images were recorded using an inverted spinning-disk confocal microscope with a 100x (NA 1.45) oil-immersion lens (Olympus).

LysoTracker imaging experiments were analyzed using NIH ImageJ software with the TrackMate analysis plug-in (53). Briefly, Laplacian of Gaussian Detector was utilized to identify LysoTracker-stained particles and a Linear Motion Linear Assignment Problem Tracker was employed to measure particle displacement and speed.

Super-resolution microscopy

A GSDIM imaging system (Leica, Wetzlar, Germany) built around an inverted microscope (DMI6000B; Leica) was used to generate super-resolution localization maps. Images were obtained using a 160x HCX Plan-Apochromat (NA 1.47) oil-immersion lens and an EMCCD camera (iXon3 897; Andor Technology). Cells were fixed with 2% paraformaldehyde-PBS (phosphate-buffered saline), permeabilized and blocked with 0.1% Triton X/50% SEA Block-PBS, and incubated with primary antibodies against TRPML1 (sc-398868, 1:50, Santa Cruz Biotechnology) and Lamp-1 (ab25245, 1:100, Abcam) or TRPML1 and RyR2 (ARR-002, 1:100; Alomone Labs, Israel). Alexa Fluor (568)- or Alexa

Fluor (647)-conjugated secondary antibodies were used for detection. During imaging, cells were kept in a thiol-based imaging solution consisting of 50 mM Tris-10 mM NaCl buffer (pH 8), 10% glucose, 10 mM mercaptoethylamine (MEA), 0.48 mg/ml glucose oxidase and 50 μg/ml catalase. Fluorophores were excited with 500 mW 532- and 642-nm lasers. Cluster size was analyzed using the open-source CellProfiler (v. 3.0.0) software package (54). Object-based analysis was used to establish colocalization of TRPML1 channels with Lamp-1 or RyR2 in super-resolution localization maps. For this analysis, we used NIH ImageJ software with the JACoP colocalization analysis plug-in, which applies a connexity analysis for image segmentation (55, 56).

Ca^{2+} sparks

SMCs were placed in a recording chamber (Warner Instruments, Hamden, CT, USA) and allowed to adhere to glass coverslips for 20 minutes at room temperature. SMCs were then loaded with Fluo-4 AM (10 μM) (Molecular Probes, Eugene, OR, USA) in the dark for 30 minutes in Ca^{2+}-free PSS, washed with Ca^{2+}-containing PSS, and incubated at room temperature for 15 minutes in the dark. Images were acquired using a spinning-disk confocal microscope (Andor) with a 100x oil-immersion objective (NA 1.45) at a frame rate of 30–60 frames per second (fps). Custom software provided by Drs. Mark T. Nelson and Adrian D. Bonev (University of Vermont) was used to analyze the properties of Ca^{2+} sparks.

Patch-clamp electrophysiology

All currents were recorded using an AxoPatch 200B amplifier equipped with an Axon CV 203BU headstage (Molecular Devices). Currents were filtered at 1 kHz, digitized at 40 kHz, and stored for subsequent analysis. Clampex and Clampfit (version 10.2; Molecular Devices) were used for data acquisition and analysis, respectively. All recordings were performed at room temperature (22°C).

Native SMCs were transferred to a recording chamber (Warner Instruments) and allowed to adhere to glass coverslips for 20 minutes at room temperature. Recording electrodes (3–5 MΩ) were pulled and polished. For perforated-patch whole-cell recordings, amphotericin B (40 μM) was included in the pipette solution to allow electrical access. Perforation was deemed acceptable if series resistance was less than 40 MΩ. STOCs were recorded in a bathing solution containing 134 mM NaCl, 6 mM KCl, 1 mM $MgCl_2$, 2 mM $CaCl_2$, 10 mM HEPES, and 10 mM glucose at pH 7.4 (NaOH). The pipette solution contained 110 mM K-aspartate, 1 mM $MgCl_2$, 30 mM KCl, 10 mM NaCl, 10 mM HEPES, and 5 μM EGTA at pH 7.2 (NaOH). STOCs were recorded from SMCs voltage-clamped at a range of membrane potentials (−60 to −20 mV). The impact of the TRPML1 activator MK6-83 (1 μM), TRPV4 agonist GSK1016790A (100 nM), and vacuolar H^+-ATPase inhibitor bafilomycin A1 (Baf-A1; 10 nM, cells pre-treated for 30 minutes) on STOCs was assessed by adding drug to the superfusing bath and recording STOCs at −30 mV. In separate experiments, STOCs were also assessed in proliferative SMCs.

Whole-cell K^+ currents were recorded using a step protocol (−100 to +100 mV in 20-mV steps for 500 ms) from a holding potential of −80 mV. Whole-cell BK currents were isolated using the selective BK channel blocker paxilline (1 μM). Current-voltage (I-V) plots were

generated using values obtained from the last 50 ms of each step. The bathing solution contained 134 mM NaCl, 6 mM KCl, 10 mM HEPES, 10 mM glucose, 2 mM $CaCl_2$, and 1 mM $MgCl_2$ at pH 7.4 (NaOH). The pipette solution contained 140 mM KCl, 1.9 mM $MgCl_2$, 75 μM Ca^{2+}, 10 mM HEPES, 0.1 mM EGTA, and 2 mM Na_2ATP at pH 7.2 (KOH).

Pressure myography

The contractility of cerebral and third-order mesenteric resistance arteries from WT and *Mcoln1*$^{-/-}$ mice was studied ex vivo in intact, cannulated and pressurized vessels. Arteries were mounted between two glass pipettes (outer diameter, 40–50 μm) in a pressure myograph chamber (Living Systems Instrumentation) and secured by nylon thread. Intraluminal pressure was controlled using a servo-controlled peristaltic pump (Living Systems Instrumentation). Pressurized vessels were visualized with an inverted microscope (Accu-Scope Inc., Commack, NY, USA) coupled to a USB camera (The Imaging Source LLC, Charlotte, NC, USA). Data were acquired using IonWizard software (version 6.4.1.73; IonOptix LLC, Westwood, MA, USA). Arteries were bathed in warmed (37°C), oxygenated (21% O_2, 6% CO_2, 73% N_2) PSS (119 mM NaCl, 4.7 mM KCl, 21 mM $NaHCO_3$, 1.17 mM $MgSO_4$, 1.8 mM $CaCl_2$, 1.18 mM KH_2PO_4, 5 mM glucose, 0.03 mM EDTA) at an intraluminal pressure of 5 mmHg. Following a 15-minute equilibration period, intraluminal pressure was increased to 110 mmHg and vessels were stretched to their approximate in vivo length, after which pressure was reduced back to 5 mmHg for an additional 15 minutes. The viability of each preparation was verified by measuring constriction in response to bath application of high extracellular [K^+] PSS, made isotonic by adjusting the [NaCl] (60 mM KCl, 63.7 mM NaCl). Arteries that showed less than 10% constriction in response to elevated [K^+] were excluded from further investigation.

Myogenic reactivity was assessed by lowering the intraluminal pressure to 5 mmHg for 15 minutes and then slowly raising it stepwise in 25-mmHg increments to 125 mmHg. Active diameter was obtained by allowing vessels to equilibrate for at least 5 minutes at each pressure, or until a steady-state diameter was reached. Following completion of the pressure-response study, intraluminal pressure was lowered to 5 mmHg and arteries were superfused with Ca^{2+}-free PSS supplemented with EGTA (2 mM) and the voltage-dependent Ca^{2+} channel blocker diltiazem (10 μM) to inhibit SMC contraction, after which passive diameter was obtained by repeating the stepwise increase in intraluminal pressure. Myogenic tone at each pressure step was calculated as myogenic tone (%) = [1 − (active lumen diameter/passive lumen diameter)] × 100.

Contraction in response to the thromboxane A_2 receptor agonist U46619 and α_1-adrenergic receptor agonist phenylephrine was assessed in cerebral and mesenteric arteries, respectively, pressurized at 20 mmHg to prevent myogenic tone development. Cumulative concentration response curves were produced through the addition of U46619 (0.01–1000 nM) or phenylephrine (0.001–100 μM) to the superfusing bath solution. Vessels were allowed to equilibrate for at least 5 minutes, or until a steady-state diameter was reached, before addition of the next concentration. Following the completion of the response curve, vessels were bathed in Ca^{2+}-free PSS solution to obtain the passive diameter. Data were

calculated as vasoconstriction (%) = [(lumen diameter at constriction − lumen diameter at baseline)/passive lumen diameter] × 100.

Relaxation in response to the nitric oxide donor sodium nitroprusside (SNP) was assessed in cerebral arteries. Vessels were pressurized to 60 mmHg to allow spontaneous development of myogenic tone. Cumulative concentration response curves were produced through the addition of SNP (0.001–100 μM) to the superfusing bath solution, and vasorelaxation was allowed to develop. Following completion of the response curve, vessels were bathed in Ca^{2+}-free PSS solution to obtain the passive diameter. Data were calculated as vasodilation (%) = [(lumen diameter at dilation − lumen diameter at baseline]/developed myogenic tone] × 100.

In vivo radio telemetry.

WT and *Mcoln1*$^{-/-}$ mice were initially anesthetized using 4–5% isoflurane carried in 100% O_2 flushed at 1 L/min, after which anesthesia was maintained by adjusting isoflurane to 1.5–2%; preoperative analgesia was provided by subcutaneous injection of 50 μg/kg buprenorphine (ZooPharm, Windsor, CO, USA). The neck was shaved and then sterilized with iodine. Under aseptic conditions, an incision (~1 cm) was made to separate the oblique and tracheal muscles and expose the left common carotid artery. The catheter of a radio telemetry transmitter (PA-C10; Data Science International, Harvard Bioscience, Inc., Minneapolis, MN, USA) was surgically implanted in the right carotid artery and secured using non-absorbable silk suture threads. The body of the transmitter was embedded in a subcutaneous skin pocket under the right arm. After a 14-day recovery period, baseline BP readings, heart rate and activity were recorded in conscious mice for 48 hours using Ponemah 6.4 (Data Science International). Parameters were measured for 20 seconds every 5 minutes.

Statistical analysis

All data, with the exception of the data describing the findings of nanoruler studies, are presented as means ± SEM (nanoruler data are presented as means ± SD). Values of “n” refer to the number of events for LysoTracker experiments; cells for super-resolution microscopy, Ca^{2+}-imaging and patch-clamp experiments; vessels for myography experiments; and animals for RT-qPCR and radio telemetry experiments. Data were compared as indicated using paired *t* tests or two-way analysis of variance using GraphPad Prism software (version 8.1.2). A P-value ≤ 0.05 was regarded as statistically significant.

Supplementary Material

Refer to Web version on PubMed Central for supplementary material.

Acknowledgments:

The authors thank Mrs. Nancy Horowitz for maintaining colonies of *smMHC*$^{Cre/eGFP}$ mice and Dr. Adrian Bonev (University of Vermont) for providing custom software for the analysis of Ca^{2+} signals.

Funding: This study was supported by grants from the National Institutes of Health (NHLBI R01HL091905, R01HL137852, and R01HL139585, NINDS RF1NS110044 and R61NS115132, and NIGMS P20GM130459 to S.E; P20GM103440, P30GM110767, and P01DK041315 to KMS; and R01HL122770 to Y.F.E.). The FACS/

FCMSRL Core at the University of Nevada, Reno School of Medicine is maintained by grants from the National Institutes of Health (P01DK041315, P20GM103440, and P30GM110767). The Transgenic Genotyping and Phenotyping Core at the COBRE Center for Molecular and Cellular Signaling in the Cardiovascular System, University of Nevada, Reno is maintained by a grant from NIH/NIGMS (P20GM130459 Sub#5451). The High Spatial and Temporal Resolution Imaging Core at the COBRE Center for Molecular and Cellular Signaling in the Cardiovascular System, University of Nevada, Reno, is maintained by a grant from NIH/NIGMS (P20GM130459 Sub#5452).

References and Notes:

1. Venkatachalam K, Wong CO, Zhu MX, The role of TRPMLs in endolysosomal trafficking and function. Cell Calcium 58, 48–56 (2015). [PubMed: 25465891]
2. Sun M et al., Mucolipidosis type IV is caused by mutations in a gene encoding a novel transient receptor potential channel. Hum Mol Genet 9, 2471–2478 (2000). [PubMed: 11030752]
3. Bargal R et al., Identification of the gene causing mucolipidosis type IV. Nat Genet 26, 118–123 (2000). [PubMed: 10973263]
4. Lindvall JM, Blomberg KE, Wennborg A, Smith CI, Differential expression and molecular characterisation of Lmo7, Myo1e, Sash1, and Mcoln2 genes in Btk-defective B-cells. Cell Immunol 235, 46–55 (2005). [PubMed: 16137664]
5. Samie MA et al., The tissue-specific expression of TRPML2 (MCOLN-2) gene is influenced by the presence of TRPML1. Pflugers Arch 459, 79–91 (2009). [PubMed: 19763610]
6. Xu H, Delling M, Li L, Dong X, Clapham DE, Activating mutation in a mucolipin transient receptor potential channel leads to melanocyte loss in varitint-waddler mice. Proc Natl Acad Sci U S A 104, 18321–18326 (2007). [PubMed: 17989217]
7. Dong XP et al., The type IV mucolipidosis-associated protein TRPML1 is an endolysosomal iron release channel. Nature 455, 992–996 (2008). [PubMed: 18794901]
8. Dong XP et al., PI(3,5)P(2) controls membrane trafficking by direct activation of mucolipin Ca(2+) release channels in the endolysosome. Nat Commun 1, 38 (2010). [PubMed: 20802798]
9. Cheng X, Shen D, Samie M, Xu H, Mucolipins: Intracellular TRPML1–3 channels. FEBS Lett 584, 2013–2021 (2010). [PubMed: 20074572]
10. Vergarajauregui S, Connelly PS, Daniels MP, Puertollano R, Autophagic dysfunction in mucolipidosis type IV patients. Hum Mol Genet 17, 2723–2737 (2008). [PubMed: 18550655]
11. Zhang X et al., MCOLN1 is a ROS sensor in lysosomes that regulates autophagy. Nat Commun 7, 12109 (2016). [PubMed: 27357649]
12. Venkatachalam K et al., Motor deficit in a Drosophila model of mucolipidosis type IV due to defective clearance of apoptotic cells. Cell 135, 838–851 (2008). [PubMed: 19041749]
13. Knot HJ, Nelson MT, Regulation of arterial diameter and wall [Ca2+] in cerebral arteries of rat by membrane potential and intravascular pressure. J Physiol 508 (Pt 1), 199–209 (1998). [PubMed: 9490839]
14. Nelson MT et al., Relaxation of arterial smooth muscle by calcium sparks. Science 270, 633–637 (1995). [PubMed: 7570021]
15. Knot HJ, Standen NB, Nelson MT, Ryanodine receptors regulate arterial diameter and wall [Ca2+] in cerebral arteries of rat via Ca2+-dependent K+ channels. J Physiol 508 (Pt 1), 211–221 (1998). [PubMed: 9490841]
16. Christensen KA, Myers JT, Swanson JA, pH-dependent regulation of lysosomal calcium in macrophages. J Cell Sci 115, 599–607 (2002). [PubMed: 11861766]
17. Xin HB, Deng KY, Rishniw M, Ji G, Kotlikoff MI, Smooth muscle expression of Cre recombinase and eGFP in transgenic mice. Physiol Genomics 10, 211–215 (2002). [PubMed: 12209023]
18. Pires PW et al., The angiotensin II receptor type 1b is the primary sensor of intraluminal pressure in cerebral artery smooth muscle cells. J Physiol 595, 4735–4753 (2017). [PubMed: 28475214]
19. Griffiths G, Hoflack B, Simons K, Mellman I, Kornfeld S, The mannose 6-phosphate receptor and the biogenesis of lysosomes. Cell 52, 329–341 (1988). [PubMed: 2964276]
20. Folling J et al., Fluorescence nanoscopy by ground-state depletion and single-molecule return. Nat Methods 5, 943–945 (2008). [PubMed: 18794861]

21. Testa I et al., Multicolor fluorescence nanoscopy in fixed and living cells by exciting conventional fluorophores with a single wavelength. Biophysical journal 99, 2686–2694 (2010). [PubMed: 20959110]
22. Bierwagen J et al., Far-field autofluorescence nanoscopy. Nano letters 10, 4249–4252 (2010). [PubMed: 20831171]
23. Schmied JJ et al., DNA origami-based standards for quantitative fluorescence microscopy. Nat Protoc 9, 1367–1391 (2014). [PubMed: 24833175]
24. Tajada S et al., Distance constraints on activation of TRPV4 channels by AKAP150-bound PKCalpha in arterial myocytes. J Gen Physiol 149, 639–659 (2017). [PubMed: 28507079]
25. Pritchard HAT, Pires PW, Yamasaki E, Thakore P, Earley S, Nanoscale remodeling of ryanodine receptor cluster size underlies cerebral microvascular dysfunction in Duchenne muscular dystrophy. Proc Natl Acad Sci U S A 115, E9745–E9752 (2018). [PubMed: 30181262]
26. Schmiege P, Fine M, Blobel G, Li X, Human TRPML1 channel structures in open and closed conformations. Nature 550, 366–370 (2017). [PubMed: 29019983]
27. Bandyopadhyay D, Cyphersmith A, Zapata JA, Kim YJ, Payne CK, Lysosome transport as a function of lysosome diameter. PLoS One 9, e86847 (2014). [PubMed: 24497985]
28. Chen CC et al., A small molecule restores function to TRPML1 mutant isoforms responsible for mucolipidosis type IV. Nat Commun 5, 4681 (2014). [PubMed: 25119295]
29. Thorneloe KS et al., N-((1S)-1-{[4-((2S)-2-{[(2,4-dichlorophenyl)sulfonyl]amino}-3-hydroxypropanoyl)-1-piperazinyl]carbonyl}-3-methylbutyl)-1-benzothiophene-2-carboxamide (GSK1016790A), a novel and potent transient receptor potential vanilloid 4 channel agonist induces urinary bladder contraction and hyperactivity: Part I. J Pharmacol Exp Ther 326, 432–442 (2008). [PubMed: 18499743]
30. Earley S, Heppner TJ, Nelson MT, Brayden JE, TRPV4 forms a novel Ca2+ signaling complex with ryanodine receptors and BKCa channels. Circ Res 97, 1270–1279 (2005). [PubMed: 16269659]
31. Mercado J et al., Local control of TRPV4 channels by AKAP150-targeted PKC in arterial smooth muscle. J Gen Physiol 143, 559–575 (2014). [PubMed: 24778429]
32. Li W et al., Neuron-specific (pro)renin receptor knockout prevents the development of salt-sensitive hypertension. Hypertension 63, 316–323 (2014). [PubMed: 24246383]
33. Kocemba J, Kawecka-Jaszcz K, Gryglewska B, Grodzicki T, Isolated systolic hypertension: pathophysiology, consequences and therapeutic benefits. J Hum Hypertens 12, 621–626 (1998). [PubMed: 9783491]
34. Brenner R et al., Vasoregulation by the beta1 subunit of the calcium-activated potassium channel. Nature 407, 870–876 (2000). [PubMed: 11057658]
35. Pluger S et al., Mice with disrupted BK channel beta1 subunit gene feature abnormal Ca(2+) spark/STOC coupling and elevated blood pressure. Circulation research 87, E53–60 (2000). [PubMed: 11090555]
36. McManus OB et al., Functional role of the beta subunit of high conductance calcium-activated potassium channels. Neuron 14, 645–650 (1995). [PubMed: 7695911]
37. Amberg GC, Santana LF, Downregulation of the BK channel beta1 subunit in genetic hypertension. Circulation research 93, 965–971 (2003). [PubMed: 14551242]
38. Amberg GC, Bonev AD, Rossow CF, Nelson MT, Santana LF, Modulation of the molecular composition of large conductance, Ca(2+) activated K(+) channels in vascular smooth muscle during hypertension. J Clin Invest 112, 717–724 (2003). [PubMed: 12952920]
39. Fernandez-Fernandez JM et al., Gain-of-function mutation in the KCNMB1 potassium channel subunit is associated with low prevalence of diastolic hypertension. J Clin Invest 113, 1032–1039 (2004). [PubMed: 15057310]
40. Fakler B, Adelman JP, Control of K(Ca) channels by calcium nano/microdomains. Neuron 59, 873–881 (2008). [PubMed: 18817728]
41. Onyenwoke RU et al., The mucolipidosis IV Ca2+ channel TRPML1 (MCOLN1) is regulated by the TOR kinase. Biochem J 470, 331–342 (2015). [PubMed: 26195823]
42. Shang S et al., Intracellular TRPA1 mediates Ca2+ release from lysosomes in dorsal root ganglion neurons. J Cell Biol 215, 369–381 (2016). [PubMed: 27799370]

43. Shen D et al., Lipid storage disorders block lysosomal trafficking by inhibiting a TRP channel and lysosomal calcium release. Nat Commun 3, 731 (2012). [PubMed: 22415822]
44. Yoshida T, Owens GK, Molecular determinants of vascular smooth muscle cell diversity. Circulation research 96, 280–291 (2005). [PubMed: 15718508]
45. Berman ER, Livni N, Shapira E, Merin S, Levij IS, Congenital corneal clouding with abnormal systemic storage bodies: a new variant of mucolipidosis. J Pediatr 84, 519–526 (1974). [PubMed: 4365943]
46. Boudewyn LC, Walkley SU, Current concepts in the neuropathogenesis of mucolipidosis type IV. J Neurochem, (2018).
47. Vaithianathan T et al., Subtype identification and functional characterization of ryanodine receptors in rat cerebral artery myocytes. Am J Physiol Cell Physiol 299, C264–278 (2010). [PubMed: 20445169]
48. Venugopal B et al., Neurologic, gastric, and opthalmologic pathologies in a murine model of mucolipidosis type IV. Am J Hum Genet 81, 1070–1083 (2007). [PubMed: 17924347]
49. Caimi L et al., Mucolipidosis IV, a sialolipidosis due to ganglioside sialidase deficiency. J Inherit Metab Dis 5, 218–224 (1982). [PubMed: 6820444]
50. Lee H, Koh BH, Peri LE, Sanders KM, Koh SD, Purinergic inhibitory regulation of murine detrusor muscles mediated by PDGFRalpha+ interstitial cells. The Journal of physiology 592, 1283–1293 (2014). [PubMed: 24396055]
51. Livak KJ, Schmittgen TD, Analysis of relative gene expression data using real-time quantitative PCR and the 2(-Delta Delta C(T)) Method. Methods 25, 402–408 (2001). [PubMed: 11846609]
52. Crnich R et al., Vasoconstriction resulting from dynamic membrane trafficking of TRPM4 in vascular smooth muscle cells. American journal of physiology. Cell physiology 299, C682–694 (2010). [PubMed: 20610768]
53. Tinevez JY et al., TrackMate: An open and extensible platform for single-particle tracking. Methods 115, 80–90 (2017). [PubMed: 27713081]
54. Carpenter AE et al., CellProfiler: image analysis software for identifying and quantifying cell phenotypes. Genome biology 7, R100 (2006). [PubMed: 17076895]
55. Lachmanovich E et al., Co-localization analysis of complex formation among membrane proteins by computerized fluorescence microscopy: application to immunofluorescence co-patching studies. Journal of microscopy 212, 122–131 (2003). [PubMed: 14629561]
56. Bolte S, Cordelieres FP, A guided tour into subcellular colocalization analysis in light microscopy. Journal of microscopy 224, 213–232 (2006). [PubMed: 17210054]

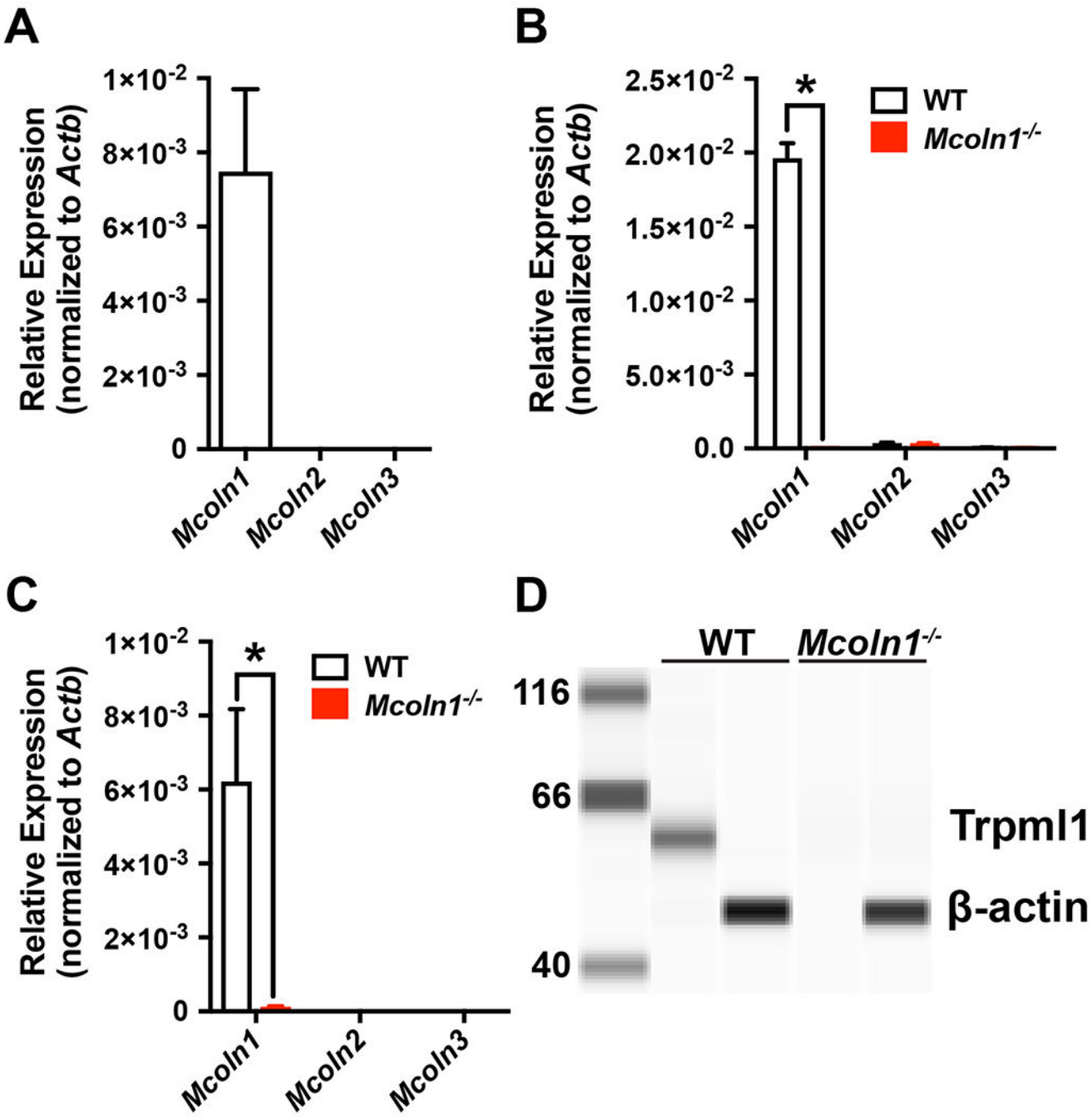

Figure 1. TRPML1 channels, are present in vascular SMCs.

A) RT-qPCR analysis of *Mcoln1, Mcoln2, and Mcoln3* mRNA expression levels in homogeneous populations of native cerebral artery SMCs. Data are normalized to *Actb*, encoding β-actin (N = 3 animals/group). B) RT-qPCR analysis of *Mcoln1, Mcoln2, and Mcoln3* mRNA expression levels in cerebral arteries from WT and *Mcoln1*$^{-/-}$ mice. Data are normalized to *Actb* (N = 3 animals/group; *P ≤ 0.05). C) RT-qPCR analysis of *Mcoln1, Mcoln2, and Mcoln3* mRNA expression levels in mesenteric arteries from WT and *Mcoln1*$^{-/-}$ mice. Data are normalized to *Actb* (N= 3 animals/group; *P ≤ 0.05). D)

Representative results of Wes protein analysis using cerebral artery lysates from WT and *Mcoln1*$^{-/-}$ mice. Samples from WT animals probed with a primary antibody against TRPML1 generated a single band at the expected molecular weight of ~60 kDa that was absent in lysates from *Mcoln1*$^{-/-}$ mice. Lysates were probed for β-actin as a loading control. Representative of 3 independent experiments using tissue from N = 3 mice. All data are shown as mean ± SEM.

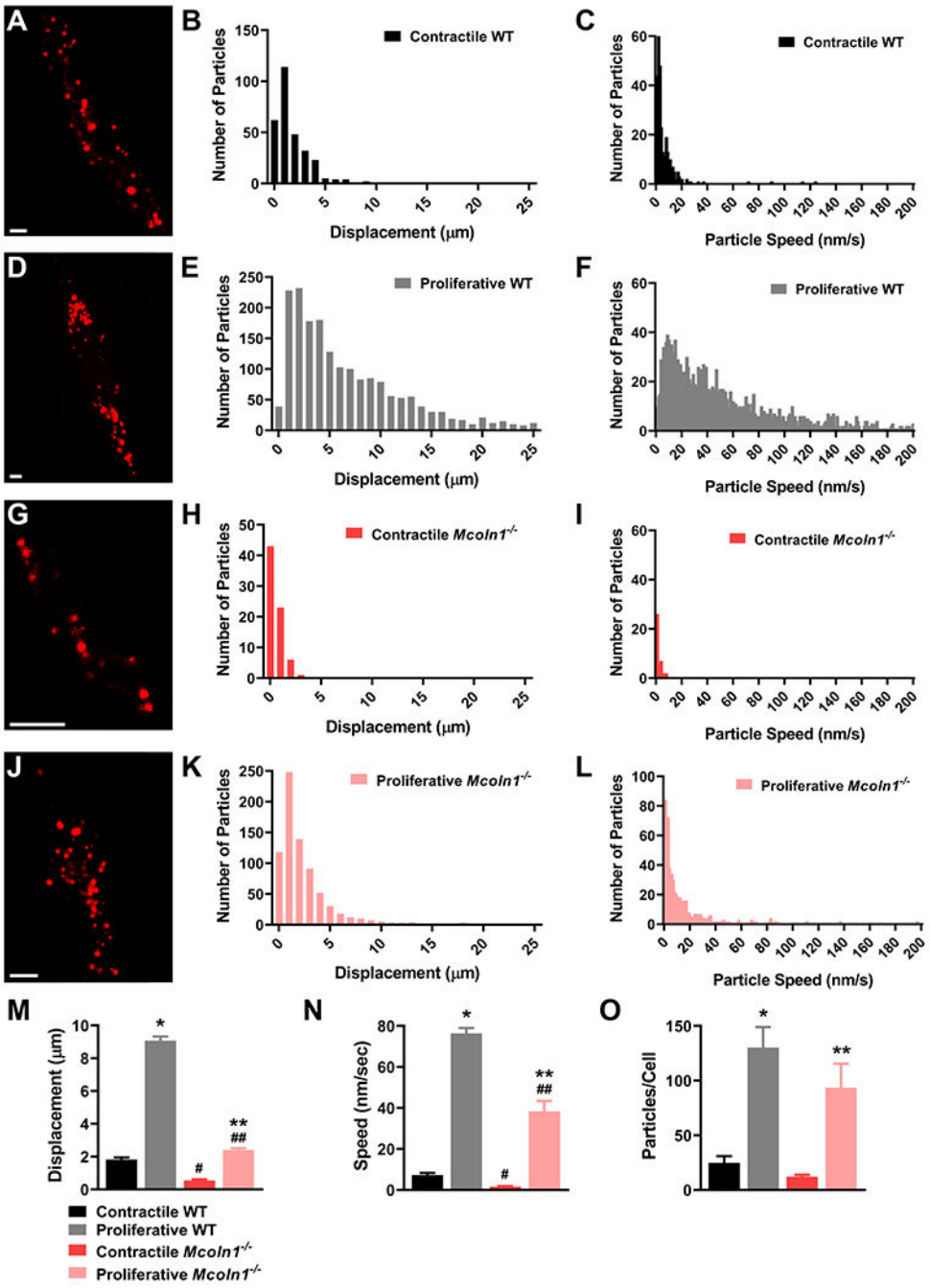

Figure 2: The majority of LELs in contractile SMCs are immobile.

A) Representative image of a native contractile cerebral artery SMC isolated from a WT mouse stained with LysoTracker. Scale bar = 10 μm. B and C) Histogram of the total displacement (B) and particle speed (C) of individual LysoTracker-labeled particles within native contractile SMCs isolated from WT mice during a 25-minute recording period. A total of 298 particles (n = 12 cells) were tracked. D) Representative image of a proliferative cerebral artery SMC isolated from a WT mouse stained with LysoTracker. Scale bar = 10 μm. E and F) Histogram of the total displacement (E) and particle speed (F) of individual

LysoTracker-labeled structures within proliferative SMCs isolated from WT mice during a 25-minute recording period. A total of 1953 particles (n = 15 cells) were tracked. G) Representative image of a native contractile cerebral artery SMC isolated from a *Mcoln1*$^{-/-}$ mouse stained with LysoTracker. Scale bar = 10 μm. H and I) Histogram of the total displacement (H) and particle speed (I) of individual LysoTracker-labeled particles within native contractile SMCs isolated from *Mcoln1*$^{-/-}$ mice during a 25-minute recording period. A total of 73 particles (n = 6 cells) were tracked. J) Representative image of a proliferative cerebral artery SMC isolated from a *Mcoln1*$^{-/-}$ mouse stained with LysoTracker. Scale bar = 10 μm. K and L) Histogram of the total displacement (K) and particle speed (L) of individual LysoTracker-labeled structures within proliferative SMCs isolated from *Mcoln1*$^{-/-}$ mice during a 25-minute recording period. A total of 748 particles (n = 7 cells) were tracked. M and N) Comparison of mean particle displacement (M) and speed (N) in contractile and proliferative SMCs isolated from WT and *Mcoln1*$^{-/-}$ mice. A total of 298 particles (n = 12 cells) from contractile SMCs isolated from WT mice, 1953 particles (n = 15 cells) from proliferative SMCs isolated from WT mice, 73 particles (n = 6 cells) from contractile SMCs isolated from *Mcoln1*$^{-/-}$ mice, and 748 particles (n = 7 cells) from proliferative SMCs isolated from *Mcoln1*$^{-/-}$ mice were tracked (*P ≤ 0.05 between Contractile WT compared to Proliferative WT; $^{\#}$P ≤ 0.05 between Contractile WT compared to Contractile *Mcoln1*$^{-/-}$; **P ≤ 0.05 between Contractile *Mcoln1*$^{-/-}$ compared to Proliferative *Mcoln1*$^{-/-}$; $^{\#\#}$P ≤ 0.05 between Proliferative WT compared to Proliferative *Mcoln1*$^{-/-}$). O) Total LysoTracker-positive particles per cell (n = 12 contractile SMCs from WT mice, n = 15 proliferative SMCs from WT mice, n = 6 contractile SMCs from *Mcoln1*$^{-/-}$ mice, and n = 7 proliferative SMCs from *Mcoln1*$^{-/-}$ mice; *P ≤ 0.05 between Contractile WT vs Proliferative WT; **P ≤ 0.05 between Contractile *Mcoln1*$^{-/-}$ vs Proliferative *Mcoln1*$^{-/-}$). All data are shown as mean ± SEM.

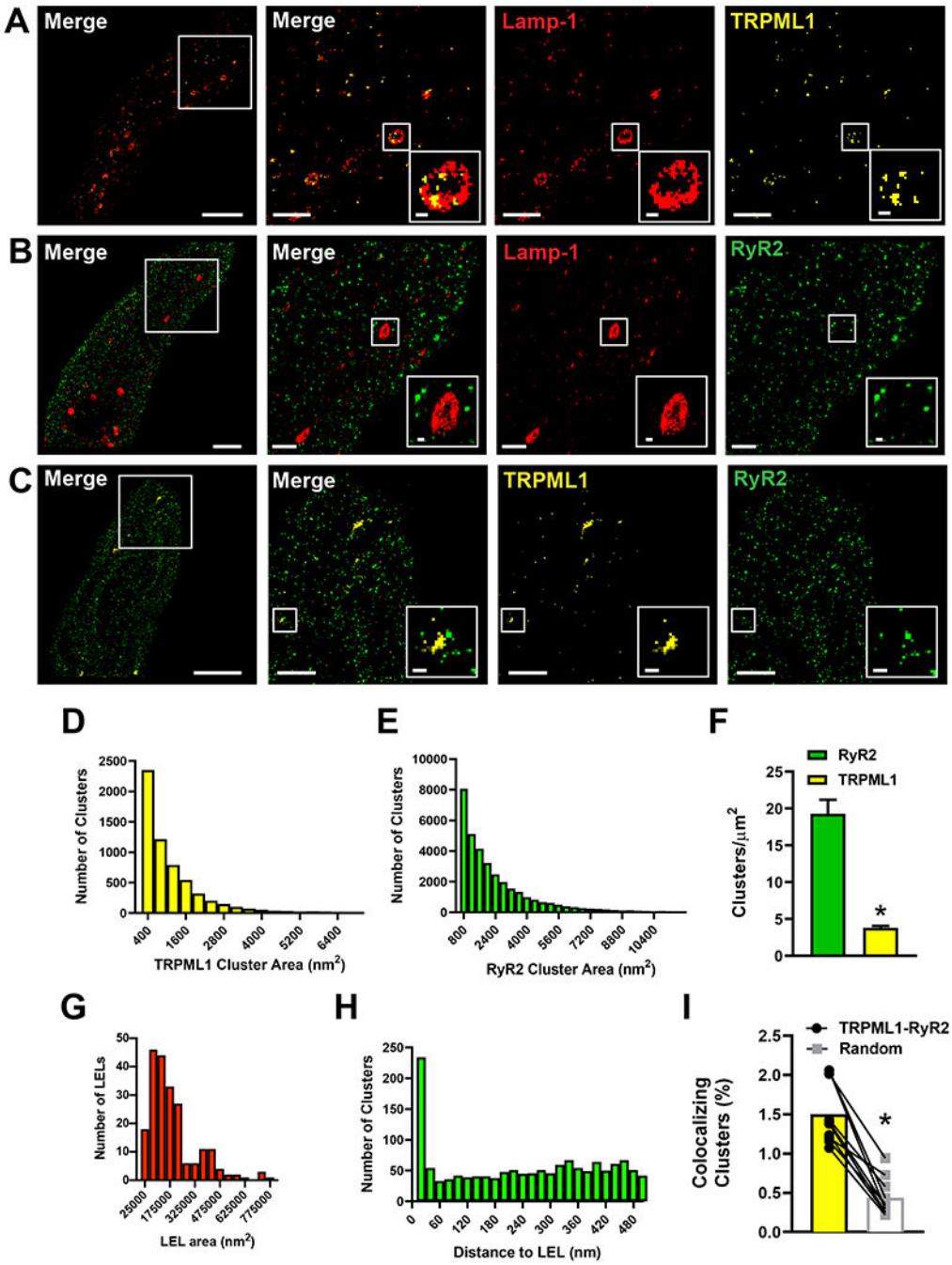

Figure 3. Super-resolution imaging demonstrates nanoscale colocalization of TRPML1 and RyR2 in native SMCs.

A–C) Representative super-resolution localization maps of native, contractile cerebral artery SMCs co-immunolabeled for Lamp-1 and TRPML1 (A), Lamp-1 and RyR2 (B), or TRPML1 and RyR2 (C). Scale bars = 3 μm. Representative of n= 8–10 cells isolated from N = 3 animals. The second column of images shows a magnified view of the region enclosed in the white boxes. Scale bars = 1 μm. Insets show magnified views of the indicated regions of interest. Scale bars = 0.1 μm. D and E) Histograms showing the distribution of the surface areas of individual protein clusters for TRPML1 (D) and RyR2 (E) (TRPML1, n = 6143

clusters; RyR2, n = 35432 clusters). F) TRPML1 and RyR2 protein cluster density (n = 19 cells from N = 6 animals/group; *P ≤ 0.05) G) Histogram showing the area distribution of Lamp-1–positive LELs (n = 216 ovoids). H) Nearest neighbor analysis showing the distance between the center of RyR2 protein clusters and the edge of Lamp-1–positive LELs (n = 1409 RyR2 protein clusters). I) Object-based analysis comparing the fraction of TRPML1 and RyR2 co-localizing clusters with the fraction of clusters that co-localize in a simulated random distribution of RyR2 protein clusters (TRPML1-RyR2, 1.51 ± 0.12 %; Random, 0.44 ± 0.07 %; n = 10 cells from 3 animals; *P ≤ 0.05). All data are shown as mean ± SEM.

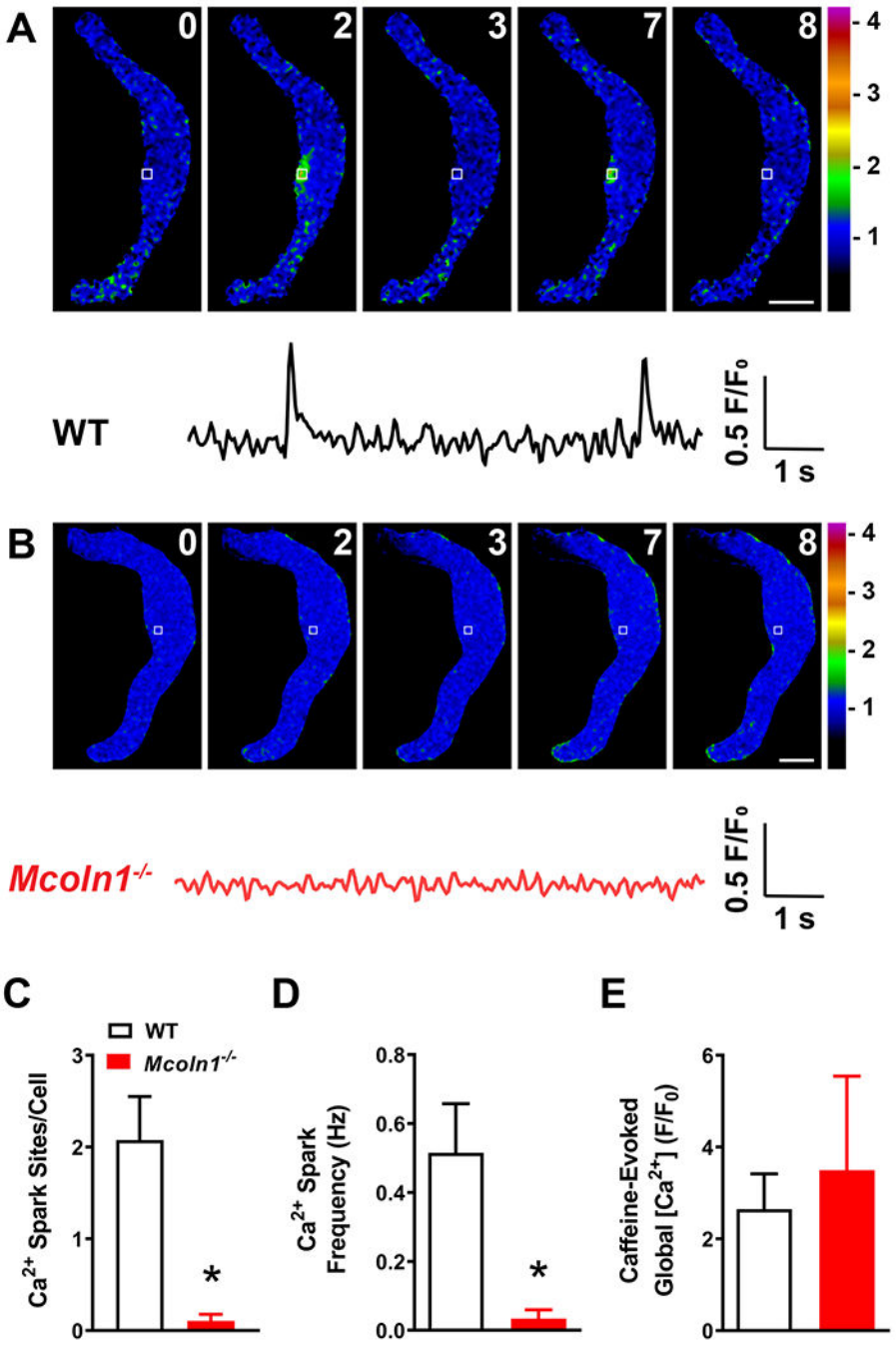

Figure 4. SMCs from *Mcoln1*$^{-/-}$ mice lack spontaneous Ca^{2+} sparks.

A) Representative time course images of a Ca^{2+} spark site (seconds; scale bar = 10 μm) and trace showing changes in fractional fluorescence (F/F_0) as a function of time for a region of interest (white box) that includes an active Ca^{2+} spark site recorded from native cerebral artery SMC isolated from a WT mouse. B) Representative time course images (seconds; scale bar = 10 μm) and trace recorded from native cerebral artery SMC isolated from a *Mcoln1*$^{-/-}$ mouse showing lack of Ca^{2+} sparks. C) Number of spontaneous Ca^{2+} spark sites per native cerebral artery SMC from WT and *Mcoln1*$^{-/-}$ mice (n = 13 cells from 4 WT

animals, n = 19 cells from 4 *Mcoln1*$^{-/-}$ animals; *P ≤ 0.05). D) Mean spontaneous Ca^{2+} spark frequency in SMCs from WT and *Mcoln1*$^{-/-}$ mice (n = 13 cells from 4 WT animals, n = 19 cells from 4 *Mcoln1*$^{-/-}$ animals; *P ≤ 0.05). E) Total SR Ca^{2+} store load in SMCs from WT and *Mcoln1*$^{-/-}$ mice, assessed by imaging changes in global intracellular [Ca^{2+}] in response to administration of caffeine (10 mM) (n = 7 cells from 3 WT mice; n = 8 cells from 3 *Mcoln1*$^{-/-}$ mice).

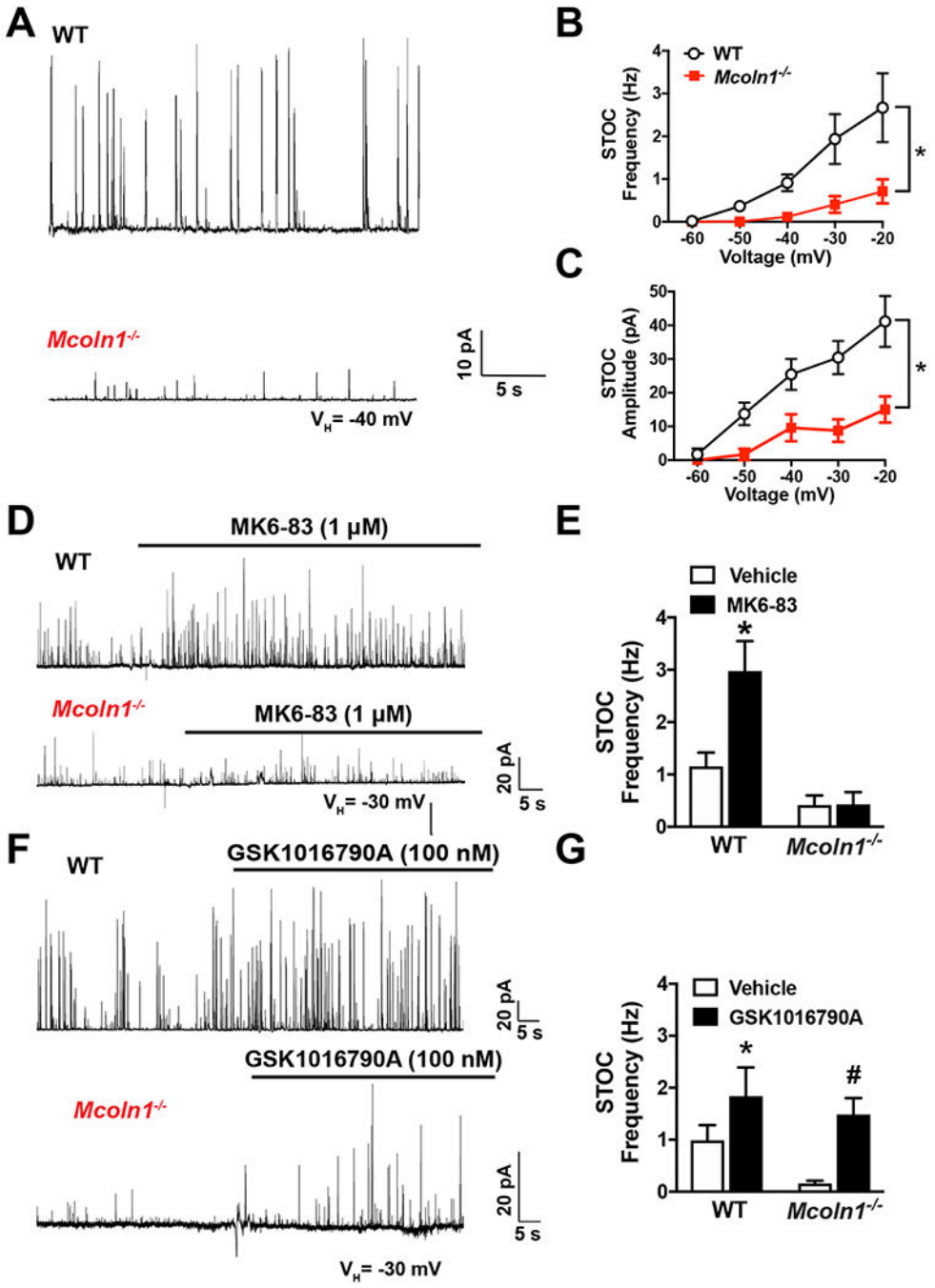

Figure 5. SMCs from *Mcoln1*$^{-/-}$ mice lack spontaneous Ca^{2+}-activated BK channel activity

A) Representative traces of STOCs recorded from voltage-clamped (−40 mV) native cerebral artery SMCs isolated from WT and *Mcoln1*$^{-/-}$ mice. B and C) Summary of mean STOC frequency (B) and amplitude (C) over a range of holding potentials (−60 to −20 mV) (n = 9 cells from 3 WT animals, n = 11 cells from 4 *Mcoln1*$^{-/-}$ animals; *P ≤ 0.05). D) Representative traces of STOCs recorded from voltage-clamped (−30 mV) SMCs isolated from WT and *Mcoln1*$^{-/-}$ mice that were treated with the selective TRPML channel activator MK6–83 (1 μM). E) Summary of the effects of MK6–83 on STOC frequency (n = 5 cells

from 3 animals for both groups; *P ≤ 0.05 compared to WT + Vehicle). F) Representative traces of STOCs recorded from voltage-clamped (−30 mV) SMCs isolated from WT and *Mcoln1*$^{-/-}$ mice that were treated with the selective TRPV4 channel activator GSK1016790A (100 nM). G) Summary of the effects of GSK1016790A on STOC frequency (n = 7 cells from 3 WT mice, n = 8 cells from 3 *Mcoln1*$^{-/-}$ mice; *P ≤ 0.05 compared to WT + Vehicle, $^{\#}$P ≤ 0.05 compared to *Mcoln1*$^{-/-}$ + Vehicle). All data are shown as mean ± SEM.

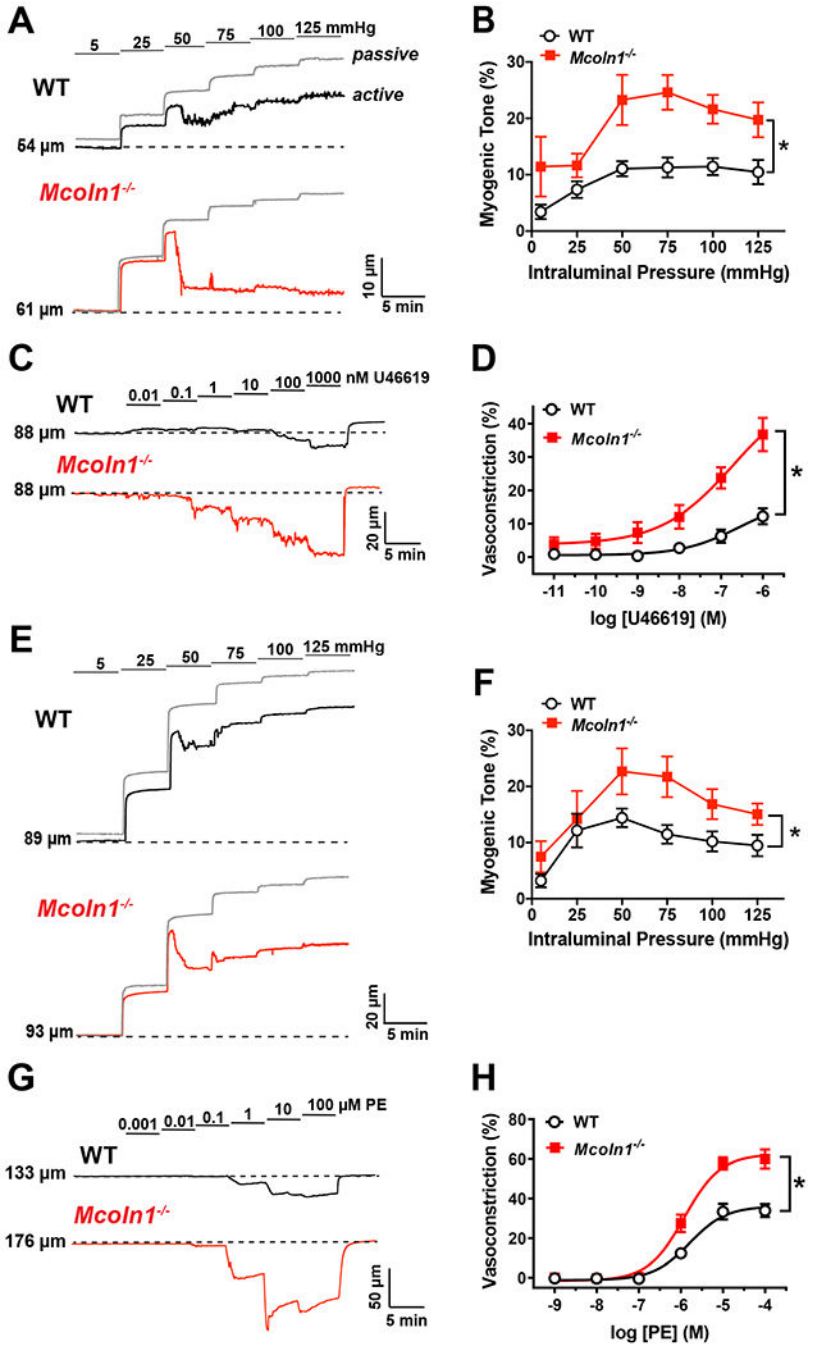

Figure 6. Resistance arteries from *Mcoln1*$^{-/-}$ mice are hypercontractile.

A) Representative recordings of pressure-induced constriction of cerebral arteries from WT and *Mcoln1*$^{-/-}$ mice. Traces show luminal diameter as a function of time in response to stepwise changes in intraluminal pressure from 5 to 125 mmHg. The diameter of the same arteries superfused with Ca^{2+}-containing and Ca^{2+}-free physiological salt solution is shown to indicate the active and passive effects, respectively, of intraluminal pressure on vessel diameter. B) Summary data showing the myogenic tone of cerebral arteries from WT and *Mcoln1*$^{-/-}$ mice as a function of intraluminal pressure (n = 9–11 arteries from 5–7 animals/

group; *P ≤ 0.05). C) Representative recordings of the thromboxane A_2 receptor agonist U46619-induced constriction of cerebral arteries from WT and *Mcoln1*$^{-/-}$ mice. D) Summary data showing the contraction produced by U46619 in cerebral arteries from WT and *Mcoln1*$^{-/-}$ mice (n = 8 arteries from 4–5 animals/group; *P ≤ 0.05). E) Representative recordings of pressure-induced constriction of mesenteric resistance arteries from WT and *Mcoln1*$^{-/-}$ mice. F) Summary data showing the myogenic tone of mesenteric arteries from WT and *Mcoln1*$^{-/-}$ mice as a function of intraluminal pressure (n = 7–9 arteries from 4–6 animals/group; *P ≤ 0.05). G) Representative recordings of α_1-adrenergic receptor agonist phenylephrine (PE)-induced constriction of mesenteric resistance arteries from WT and *Mcoln1*$^{-/-}$ mice. H) Summary data showing the contraction produced by PE in mesenteric arteries from WT and *Mcoln1*$^{-/-}$ mice (n = 7–8 arteries from 3 animals/group; *P ≤ 0.05). All data are shown as mean ± SEM.

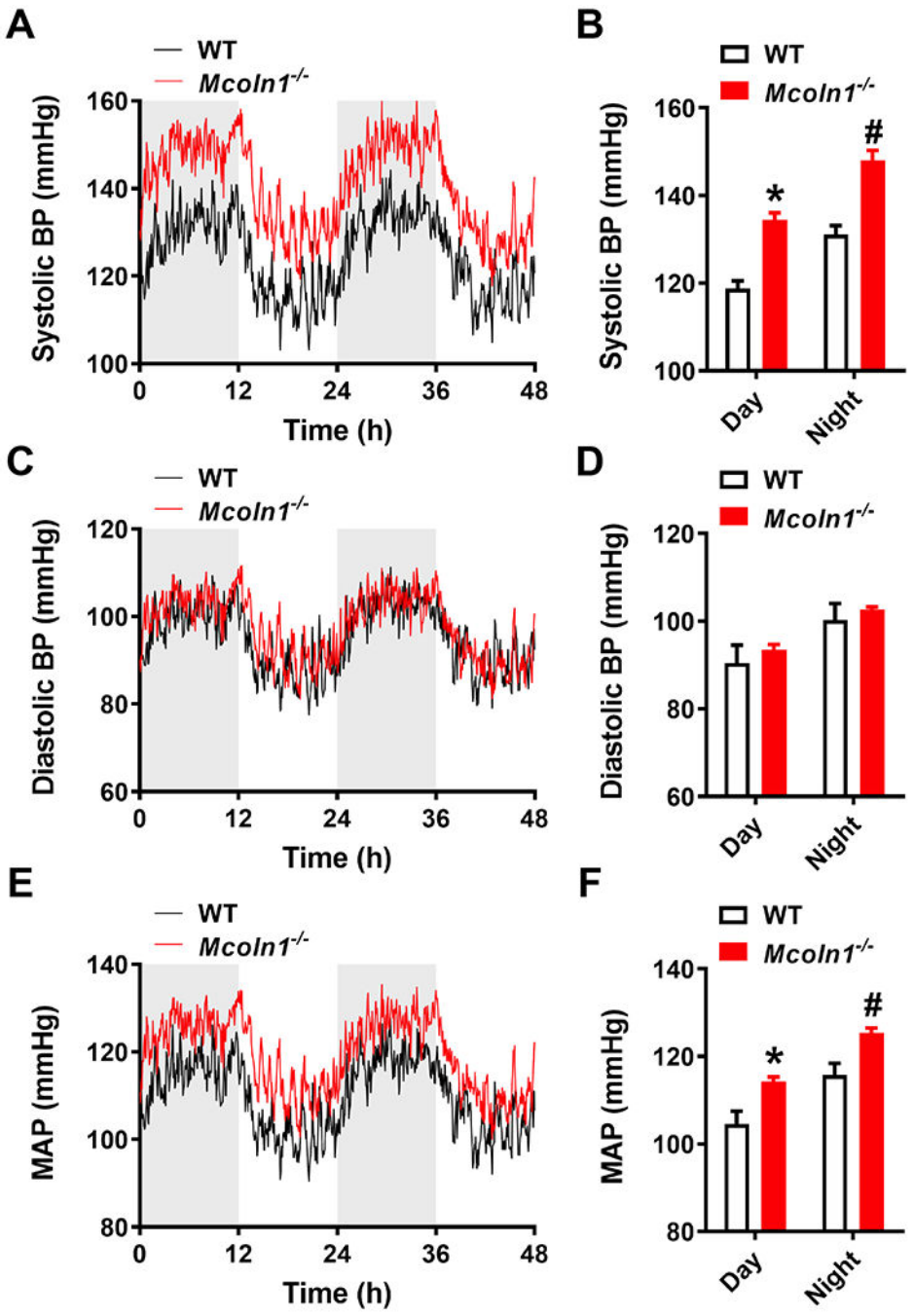

Figure 7. *Mcoln1*$^{-/-}$ mice are spontaneously hypertensive.

A) Averaged systolic BP measurements over a 48-hour period in conscious radiotelemetered WT and *Mcoln1*$^{-/-}$ mice. Shaded regions depict night cycles. B) Mean systolic BP of WT and *Mcoln1*$^{-/-}$ mice during day and night cycles (n = 7 for WT, n = 5 for *Mcoln1*$^{-/-}$; *P ≤ 0.05 compared to WT day, $^{\#}$P ≤ 0.05 compared to WT night). C) Averaged diastolic BP measurements over a 48-hour period in conscious radio telemetered WT and *Mcoln1*$^{-/-}$ mice. D) Mean diastolic BP in WT and *Mcoln1*$^{-/-}$ mice during day and night cycles (n = 7 for WT, n = 5 for *Mcoln1*$^{-/-}$). E) Averaged MAP measurements over a 48-hour period in

conscious radio telemetered WT and *Mcoln1*$^{-/-}$ mice. F) Mean MAP in WT and *Mcoln1*$^{-/-}$ mice during day and night cycles (n = 7 for WT, n = 5 for *Mcoln1*$^{-/-}$; *P ≤ 0.05 compared to WT day, $^{\#}$P ≤ 0.05 compared to WT night). 48-hour recordings are shown as mean; bar graphs are shown as mean ± SEM.